Temperature Homogenization with Tungsten Absorber on X-Ray Mask

by

Huiying Li

Submitted to the Department of Electrical Engineering and Computer Science

in Partial Fulfillment of the Requirements for the Degrees of

Bachelor of Science in Electrical Science and Engineering

and Master of Engineering in Electrical Engineering and Computer Science

at the Massachusetts Institute of Technology

May 1994

Author_____
Department of Electrical Engineering and Computer Science
May 18, 1994
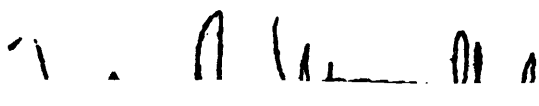
Certified by_____
Henry I. Smith
Professor
Thesis Supervisor
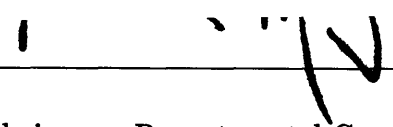
Accepted by_____
F. R. Morgenthaler
Chairman, Departmental Committee on Undergraduate Theses

Temperature Homogenization with Tungsten Absorber on X-Ray Mask

by

Huiying Li

Submitted to the
Department of Electrical Engineering and Computer Science

May 18, 1994

In Partial Fulfillment of the Requirements for the Degrees of
Bachelor of Science in Electrical Science and Engineering
and Master of Engineering in Electrical Engineering and Computer Science

Abstract

Tungsten absorber with low and stable stress is critical to the applicability of X-ray mask technology for producing submicrometer features. This thesis focuses on reducing stress non-uniformity created by plasma heating through a new approach called helium backside temperature homogenization. This technique successfully produces absorber with uniform stress. Although low stress absorber has been obtained, the reproducibility of the stress is poor.

Thesis Supervisor: Henry I. Smith
Title: Professor

Acknowledgments

Contents

List of Figures

List of Tables

Chapter 1

Introduction

As the trend for ever smaller device dimensions continues in VLSI chip manufacture, X-ray lithography is well positioned to be the technology of the future. Compared to optical lithography, X-ray lithography has the advantage of higher resolution; compared to electron/ion beam writing, X-ray lithography has higher throughput [24]. It remains to be determined if optical lithography will be practical for feature size of 0.25 micron and below, while sub $100nm$ features have been successfully produced using X-ray. Electron beam direct write is good for mask generation; however, it is far more expensive than X-ray to print large volumes of wafers. The distortion in the X-ray mask membrane may be a major obstacle to the general adoption of X-ray lithography.

Since X-ray lithography is a one-to-one replication technique, the quality of the replicated patterns depends critically on pattern-placement accuracy in the X-ray masks. In fact, it is one of the most serious issues in X-ray lithography. Therefore, it is important to achieve precise control of the absorber film stress, since this stress can cause a pattern displacement error of the absorber on the thin membrane. For a minimum feature size of $100nm$ and below, the absorber should have less than $5 \times 10^7 dynes/cm^2$ internal stress [13].

Many studies have been done to produce a low stress absorber for the X-ray mask. One area that has not received proper attention is the non-uniformity in absorber stress caused by a thermal gradient in the membrane during absorber deposition

process. Non-uniform stress can cause pattern displacement errors depending on their positions on the membrane. Therefore, following the techniques used in previous studies on thermal effects in X-ray masks for synchrotron irradiation and reactive ion etching [5] [17], helium is used as a cooling gas for the membrane during the absorber deposition process.

This method is called helium backside temperature homogenization (HBTH), where helium is introduced into a gap between the back of the membrane and a massive heat sink. The high conductivity of this gas provides a very efficient homogenization mechanism. The membrane temperature is controlled by the equilibrium between the absorbed power input and the heat removed by conduction through the helium to the heat sink surface. To keep the temperature constant, the heat sink temperature is separately controlled.

In this work, we characterize the HBTH and related technologies. In chapter 2, we detail the physical background involved in HBTH, i.e. X-ray lithography, absorber and RF sputtering, and stress. In chapter 3, we analyze the effects of deposition conditions. In chapter 4, we introduce the HBTH experimental setup. In chapter 5, we summarize the measurement techniques and analysis of the results. Finally in chapter 6, possible future works are suggested.

Chapter 2

Physical Background

In this chapter, I want to discuss the basic technologies and concepts involved in this thesis.

2.1 X-ray Lithography

X-ray lithography is a technique to print patterns onto substrates. An X-ray mask is made of a transmissive membrane and patterned absorber, as depicted in Figure 2.1.

The mask is held in close proximity of the wafer $(0 - 50\mu m)$ [6]. X-rays are shone through the thin membrane and expose the resist in the clear areas. To achieve high contrast printing, the absorber must have high X-ray attenuation.

SiN_x is a good membrane material because it has high X-ray transparency. The mask membrane used in the NanoStructures Laboratory at the Massachusetts Institute of Technology for x-ray masks is 31mm in diameter and $1.0\mu m$ thick Si-rich SiN_x whose fabrication process of the membrane has been developed at MIT [16].

Mask can be fabricated with an additive process or a subtractive process. The additive process usually involves electroplating Au. This process has the advantage of producing low stress film. The disadvantages are Au has a large thermal expansion coefficient and plating is a wet chemical process, which is more prone to defects.

In the substrative process, W or Ta is deposited by sputtering. Ta has better dry etching characteristics, while W has higher density than that of Ta. Suzuki
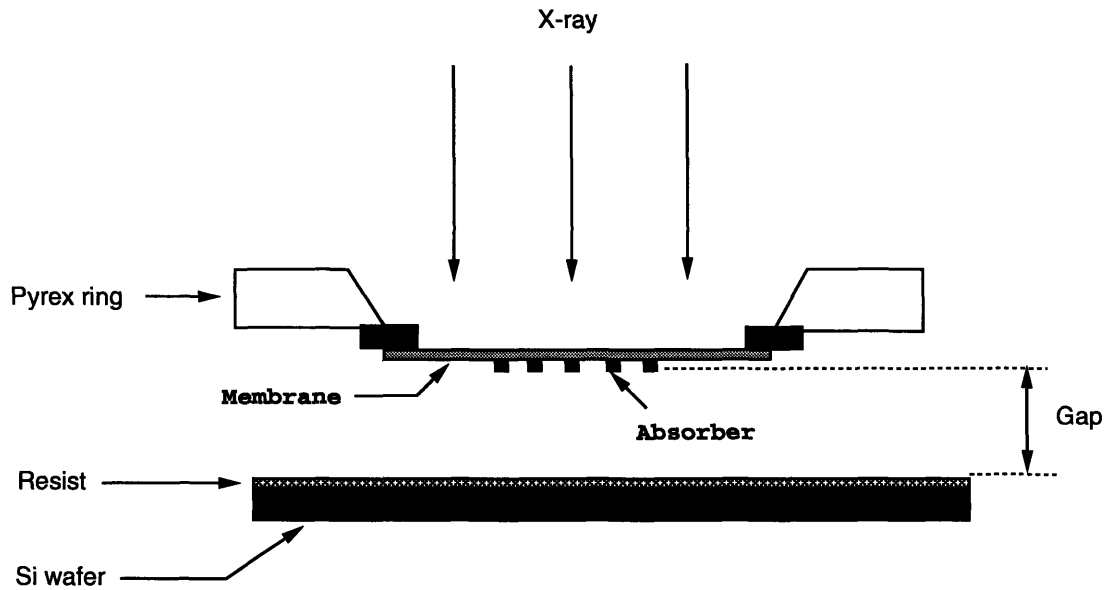
Figure 2-1: X-ray Lithography Mask

has developed a more simplified x-ray mask fabrication with a subtractive tungsten absorber pattern fabrication process using a single-layer resist as an etching mask [23].

2.2 Tungsten as Lithography Absorber

Tungsten can replace gold as a good X-ray absorber because it has high X-ray absorption, has a close thermal expansion match with membrane materials, and can be patterned with a subtractive process.

The thickness of the absorber is chosen to give $10dB$ or more X-ray attenuation at the wavelength used. At X-ray wavelength $\lambda = 1.3nm$, $200nm$ Au or $250nm$ W absorbers give $10dB$ attenuation [13].

Since the X-ray mask undergoes temperature changes during the various processes involved in lithography, it is desirable to have matched thermal expansion coeffients on film layers to minimize pattern degradation. Tungsten's thermal expansion coefficent $(4.3 \times 10^{-6} K^{-1})$ best matches the coefficient of the membrane ($2.7 \times 10^{-6} K^{-1}$), when
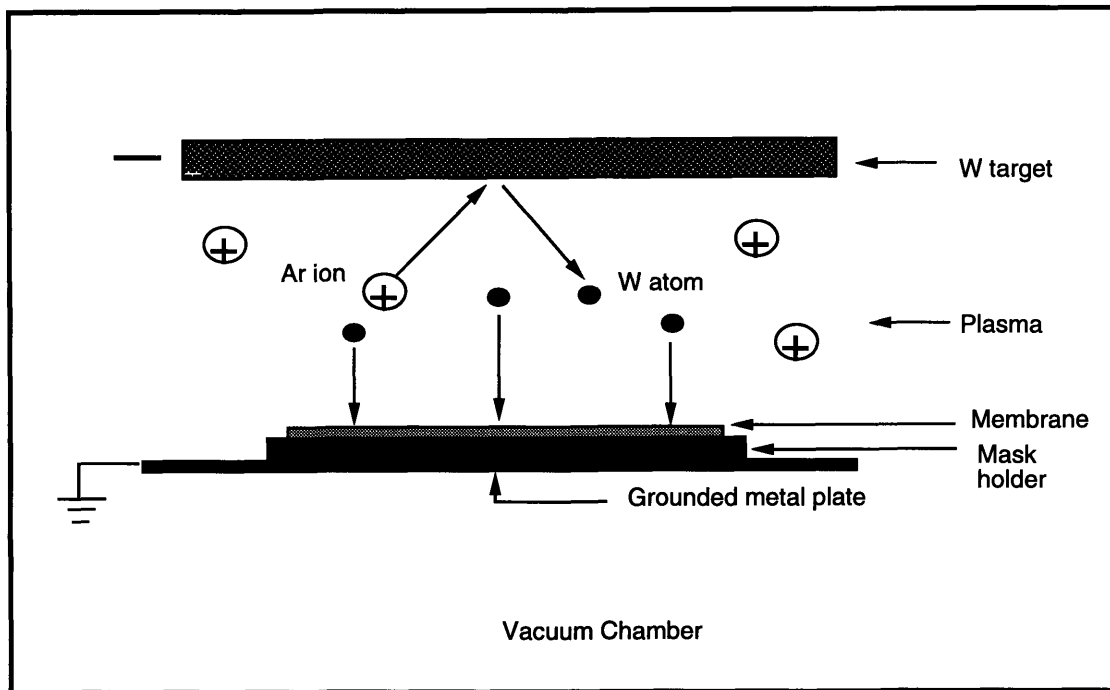
Figure 2-2: RF Sputtering Deposition of W on X-ray Mask

compared to Au $(14.3 \times 10^{-6} K^{-1})$ and Ta $(6.5 \times 10^{-6} K^{-1})$ [13].

Furthermore, tungsten can be patterned by reactive-ion-eching (RIE). RIE is a "dry" process because the etching takes place in a plasma, not a "wet" chemical solution.

2.3   Sputter Deposition of Tungsten

Tungsten (W) can be deposited by evaporation or sputtering. For absorber thicknesses of interest here, 0.1 to $1\mu m$, evaporation is not practical. Therefore sputtering is the W absorber fabrication technique of choice because of its superior deposition rate, $20.8 nm/min$ at $200W$ RF power.

The basic theory of sputtering is illustrated in Figure 2.2. A large negative self bias

voltage appears on a circular W target. Therefore, the Ar ions generated in the RF plasma are accelerated to the W target. When the heavy Ar ions reach the W target, they remore or "sputter" W atoms from the target by exchange of kinetic energy and momentum. Some of these W atoms are collected on the substrate (membrane) and form a thin W absorber layer.

A serious problem in sputtering tungsten is the high stress in the deposited film. For fabrication of stable long term x-ray masks, film stress must be controlled to the required level of $1 \times 10^8 dyn/cm^2 (10 MPa)$ [13].

2.4 Absorber Stress

Stress in films is directly related to mask distortion. To control the distortion we need low stress absorber film because the distortion becomes smaller as the absorber stress decreases.

There are two major components of stress in a thin film, intrinsic stress and thermal stress [3]. The intrinsic stress results from the structure and growth of films. It depends on the conditions of the deposition process, which is explained in chapter 3. Thermal stress is due to the difference in the thermal-expansion coefficients of the film and the substrate and is given by

$$S_{Th} = (\alpha_F - \alpha_s)\Delta T E_F \qquad (2.1)$$

where α_F and α_s are the average coefficients of expansion for W film and membrane, ΔT is the difference in membrane temperature during W deposition and at measurement, and E_F is the Young's modulus of the W film [13].

When the intrinsic stress is controlled at a low level, thermal stress can become the main contribution to stress. To minimize thermal stress, we want the thermal expansion coefficients of the films to match. Furthermore, if there is a gradient in temperature on the membrane during deposition, there will also be a corresponding gradient in stress on the membrane. The elimination of this difference in thermal stress is the focus of this work.

Chapter 3

Absorber Fabrication via Sputter Deposition

3.1 Sputter Deposition of Tungsten

Tungsten is deposited by RF sputtering as discussed in Chapter 2. To guarantee excellent adhesion to the substrate, a thin chrome adhesion layer, 5 to $15nm$ is sputtered on the membrane before W sputtering. Cr is also useful as an etching stop in the RIE absorber patterning step of mask fabrication process. To summarize, the process of W fabrication involves three steps. First, a membrane is cleaned with a chemical solution of NH_4OH and H_2O_2 (RCA clean) to remove organic contamination . Second, a thin Cr adhesion layer is sputtered on the membrane. Finally, $500nm$ of W is sputtered. $500nm$ W corresponding to 20dB contrast. In an actual X-ray mask only $200 - 250nm$ of W is required. The final result is shown in Figure 3.1.

A serious problem in sputtering tungsten is the high stress in the deposited film. For fabrication of X-ray masks, film stress must be controlled to the required level as low as $1 \times 10^8 dyn/cm^2 (10MPa)$. Even though results from the efforts to make low stress tungsten are mixed, models for the origin of stress have been generally accepted. The tensile stress of the film can be modeled using the interatomic forces acting on the grain boundary [8]. Compressive stress is explained as the result of atomic peening action.

250nm W 10dB

10nm Cr

1000nm SiNx
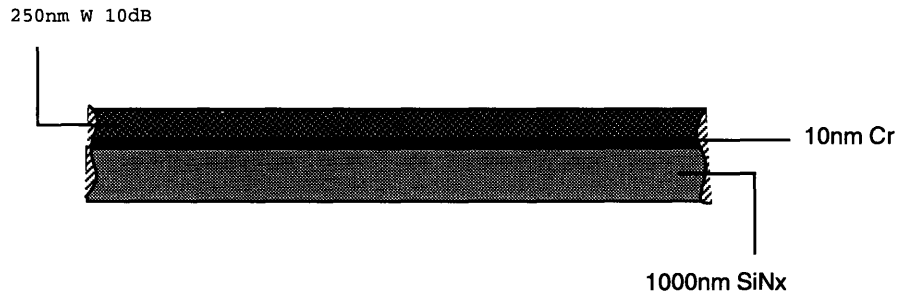
Figure 3-1: X-ray Membrane and Absorber Layers

3.2 Deposition Conditions and Absorber Stress

To minimize distortions in an X-ray mask, intrinsic stresses in the absorber films must be low and reproducible. All the parameters related to sputtering conditions can potentially have an impact on the absorber stress. As a result, the conditions such as working gas (Ar) pressure, electric power, substrate temperature, base pressure, and geometry of the vacuum chamber have been investigated in many works.

For example, Kadela observed that "stress in tungsten layers was heavily dependent on the substrate, layer thickness, deposition rate and argon pressure and on the electrical power used for sputtering" [9]. This statement made clear that many parameters affect the W film stress. Even though a set of optimized parameters are found for one facility, they won't be the same under new conditions or a different facility. Nonetheless, it is beneficial to have some general idea of each parameter's relationship with stress when finding the optimal parameters for a new experiment. In the following paragraphs, I summarize some of the relationships.

Working Gas Pressure Working gas pressure strongly influences the stress of the sputter-deposited film [7]. The stress shifts in the tensile direction when the pressure is increased [13] [25]. The stress transition from compressive to tensile is characterized by an abrupt slope[2] [13]. This abrupt transition is one of the difficulties in precisely

15

controlling the W film stress with good reproducibility and obtaining stress stability.

The general agreement on the stress and pressure relationship ends here. The exact shape of stress versus pressure curve varies depending on the vacuum system and sputtering conditions.

Base Pressure Base pressure is the vacuum pressure before deposition is initiated. A low base pressure can represent a good system cleanness. Kola claimed that a low base pressure ($P = 1 \times 10^7 torr$) is necessary to produce stable α-phase W [12].

Substrate Temperature Chaker found that "the magnitude of the compressive stress decreases almost linearly with temperature, with a slope $\delta stress/\delta T$ of about $50MPa$ per $100^\circ C$" [2]. Ku stated that a substrate temperature of $200^\circ C$ is necessary to produce stable low stress W with the MRC8620 RF sputtering system [13]. Therefore, $200^\circ C$ is chosen as the temperature for the sputter depositions in this work.

Stress Reproducibility There are different accounts in this area. Some have achieved reproducible low stress absorbers, others have only partial or no success.

Yabe stated that smooth stress-free amorphous high density W absorber film was obtained by optimizing parameters such as gas pressure, N_2 content in the working gas, DC power density, and annealing temperature. The reproducibility of the film stress was about $\pm 50MPa$ or $5 \times 10^8 dynes/cm^2$ [25]. Kola maintains that stress reproducibility is better at low power because higher plasma heating of the substrates and higher deposition rates give the atoms less time to find stable lattice sites [12]. Itoh and Hori found that it is difficult to precisely control the W film stress with good reproducibility and obtain stress stability because the stress of a sputter-deposited film varies just from a slight change in the working gas pressure. They said the stress of tungsten absorber, however, can be reduced to as low as $5 \times 10^7 dyn/cm^2$ with ion implantation [7].

My results show that reproducing low stress W absorber is very difficult. Even though the Ar pressure in the sputtering chamber is controlled within $\pm 0.01 mtorr$

which is below the level of $\pm 0.05 mtorr$ as specified by Kola [12]. So, there must be other parameters that contribute to the poor reproducibility.

3.3   Other Techniques of Stress Reduction

People have tried different methods to reduce W stress post deposition. Most of the schemes involve annealing and/or ion implantation. They are very successful as some results show. In the following chapters, we develop a new method called helium backside temperature homogenization, which aims to produce low and uniform stress during deposition.

Annealing   Yabe found that annealing shifts the film stress in the tensile direction [25]. This suggests that stress can be compensated by properly controlling the annealing process. Chaker successfully used rapid thermal annealing (RTA) process as a post deposition stress correction [2]. Kanayama combined ion implantation and annealing, and got similar results [10].

Ion Implantation   Itoh and Hori performed Ne, Ar, Kr, Si ion implantations to modify the absorber stress. They concluded that ion implantation is effective to relieve the stress of W. Their explanation for the stress reduction is that the implanted layer prevents the films from oxygen absorption at the grain boundary and also from any decrease in the intercolumnar gaps. The volume expansion of the implanted layer closes the intercolumnar gaps of the films [7].

Kanayama used ion bombardment as a stress-compensation technique in X-ray absorber layers and found that compressive stress of $10^{10} dyn/cm^2$ can be completely compensated to less than $5x10^6 dyn/cm^2$ in $0.4\mu m$ thick WNx layers by ion bombardment at an elevated temperature ($300^\circ C$) [10].

17

Chapter 4

Helium Backside Temperature Homogenization (HBTH)

This chapter introduces the helium backside temperature homogenization as a method to produce uniform stress tungsten absorber for X-ray masks. In the following sections, we first discuss why HBTH is needed. Then, we review the pressure dependence of helium heat conductivity and present the HBTH experimental set up and control. Finally, we calculate the resulted temperature profile on the membrane based on a heat transfer model.

4.1 Motivation

The plasma produced during RF sputterring has sufficient power to raise the temperature of the substrate material. In my experiments without HBTH the MRC 8620 sputter system raises the temperature of the heat sink from $28^\circ C$ to $48^\circ C$ by plasma heating alone. Since the Si rim on the mask, the Pyrex supporting ring, and the Aluminum holder have large thermal mass, they act like a heat sink. Moreover, the thin membrane is a very poor conducting material. So the plasma heating not only raises the temperature of the membrane, but also produces a non-uniform temperature profile on the membrane. The center of the membrane has a higher temperature than the edge of the membrane. Consequently the thermal stress at the center is also

membrane   Si Rim

Gap

Al heat sink   Pyrex glass
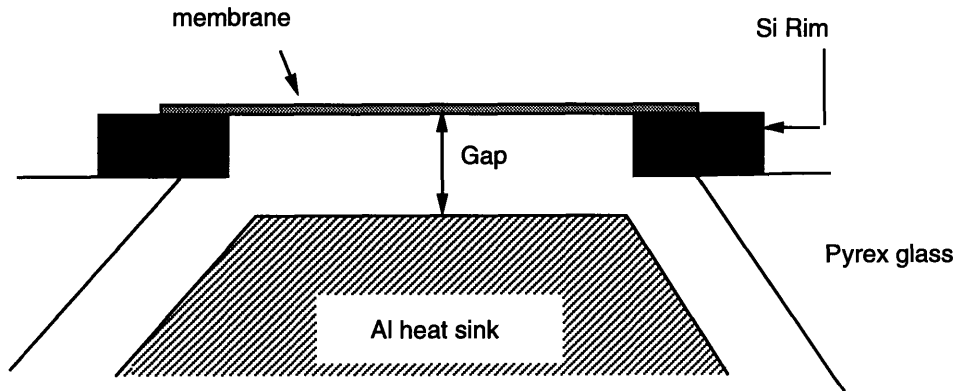
Figure 4-1: HBTH Setup

higher.

To avoid the temperature gradient caused by plasma heating during the deposition process, we applied a temperature homogenization method with helium as a cooling gas. Because helium has high thermal conductivity, it can quickly dissipate the heat from plasma, maintain a constant temperature on the entire membrane, and eliminate the non-uniform thermal stress.

Interestingly, gas cooling has been used successfully in the reactive ion etching (RIE) [17], X-ray synchrotron radiation [5] on membranes, and ion implantation process [11] [19] [20] on silicon wafers. However, no work has yet been done with gas cooling of membranes during sputtering deposition to address the problem of non-uniform stress caused by plasma heating.

4.2 HBTH Aparatus

The design considerations and actual setup for HBTH are explained in this section. The basic parameters that need to be determined are gap dimensions and helium pressure, as shown in Figure 4.1. In addition, a control mechanism is needed to regulate the helium pressure and mask holder temperature.

19

4.2.1 Gap and Pressure

The conductivity of helium gas depends on the size of the gap at the back of the membrane and the helium pressure. At low pressures, the conductivity of helium increases with pressure; at high pressure, the conductivity reaches a constant value which is independent of the pressure. The pressure is considered to be low if the mean free path of helium gas molecules is greater than the gap between two heat conducting surfaces [4]. In the HBTH case, the two surfaces are the membrane and the surface of the heat sink.

Mean free path, denoted as l, of He gas molecules at 25^oC and $1torr$ is $1.47 \times 10^{-1}mm$. At other temperature and pressure, l varies as $\sqrt{T}/p$, where T is temperature and p is helium pressure [11]. From this relationship, l at 200^oC and $5torr$ is $3.86 \times 10^{-2}mm$. If we set the gap at $1mm$, then $5torr$ or more is definitely in the high pressure region.

At high pressures, the conductivity of He becomes a constant and the heat transfer is given by,

$$E/A = k(T_m - T_{mh})/g \tag{4.1}$$

where E is heat transfer rate (power transfer) from hot membrane surface to heat sink plate, g is the gap between the two plates, k is the heat conductivity of helium, which is a constant of $1.436mW/cmC$ [4], T_m is the temperature of the membrane, T_{mh} the temperature of the heat sink. From Equation 4.1, helium transfers $14.36mw/cm^2$ by conduction if the temperature differential is 1^oC and the gap is $1mm$.

Membrane Deflection   Helium pressure within the gap is set at $5torr$ as determined above. This pressure is higher than the Ar pressure ($\leq 20mtorr$) in the chamber, so the membrane is slightly bulged up. The deflection of the membrane can be calculated using the following formula,

$$p = \frac{4t\sigma_o}{r^2}h + \frac{8t}{3r^4}\frac{E}{1-\gamma}h^3 \tag{4.2}$$

for a membrane with radius r, deflection height h, film thickness t, intrinsic stress σ_o, and bulk modulus $E/1 - \gamma$ at a pressure differential p [1]. The calculated membrane deflection is $100\mu m$ using data from Gabrielle Owen [18]. This deflection is low enough to maintain a constant thermal transfer.

4.2.2 Experimental Setup

A schematic layout of the setup is shown in figure 4.2. The setup consists of a temperature controlled aluminum (Al) heat sink, a helium pressure control loop, and two vacuum isolation valves (valve one and valve two).

The heat sink's temperature is maintained at $200^\circ C$ during sputtering. It is heated for at least an hour before deposition so that the mask glass supporting ring and the Si rim on the mask achieve thermal equilibrium with the Al holder.

The gap between the back side of the mask membrane and the aluminum holder is $1mm$. While the vacuum chamber is being pumped down to base pressure, valve one is closed and valve two is open so the gap behind the membrane also achieves a vacuum. When the desired base pressure is obtained and the deposition begins, valve two is closed and valve one is open to allow helium to flow into the gap.

The helium pressure and flow control loop consists of a control valve, a programmed controller, and a pressure gauge. The controller gets pressure measurement from the pressure gauge and then adjusts the position of the control valve so that the helium pressure stays at the pre-set $5torr$ pressure. This pressure is maintained throughout the deposition process.

This setup makes sure the gap behind the membrane is filled with helium at a constant pressure and the heat sink's temperature is constant. The temperature on the membrane is therefore homogenized. Figure 4.3 summarizes the improvement that is possible with HBTH [15]. A more detailed mathematical model for the temperature profile on the membrane is discussed in the next section.
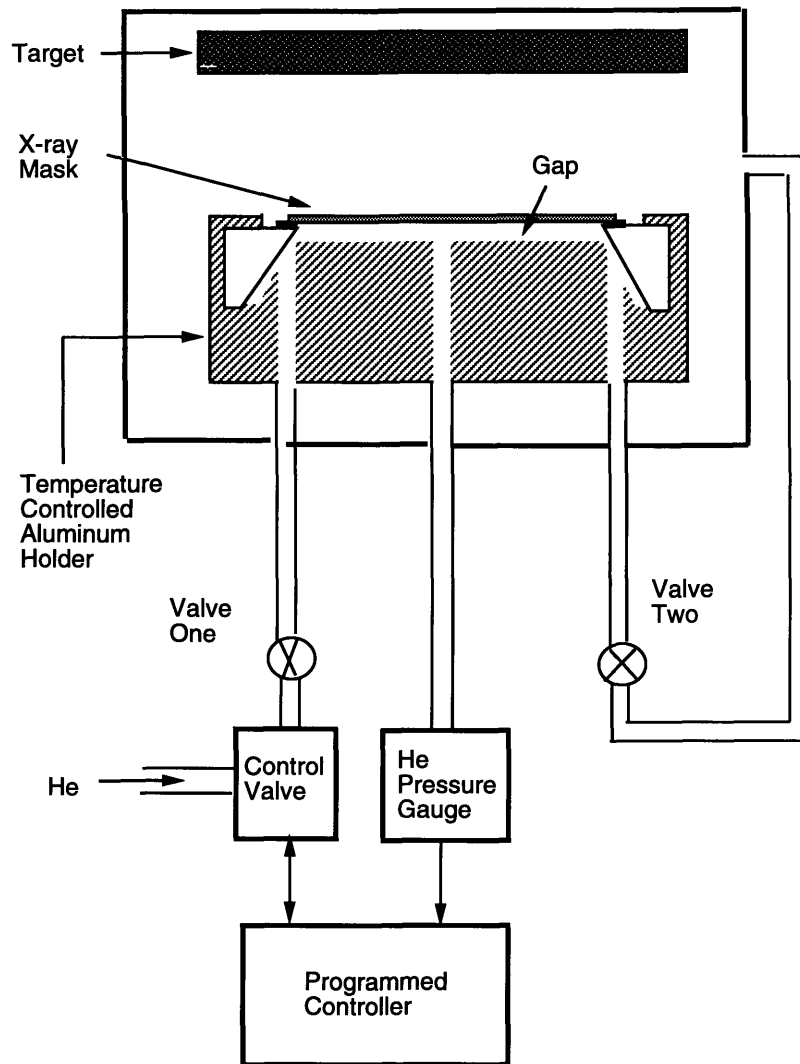
Figure 4-2: Schemetics of HBTH and Control
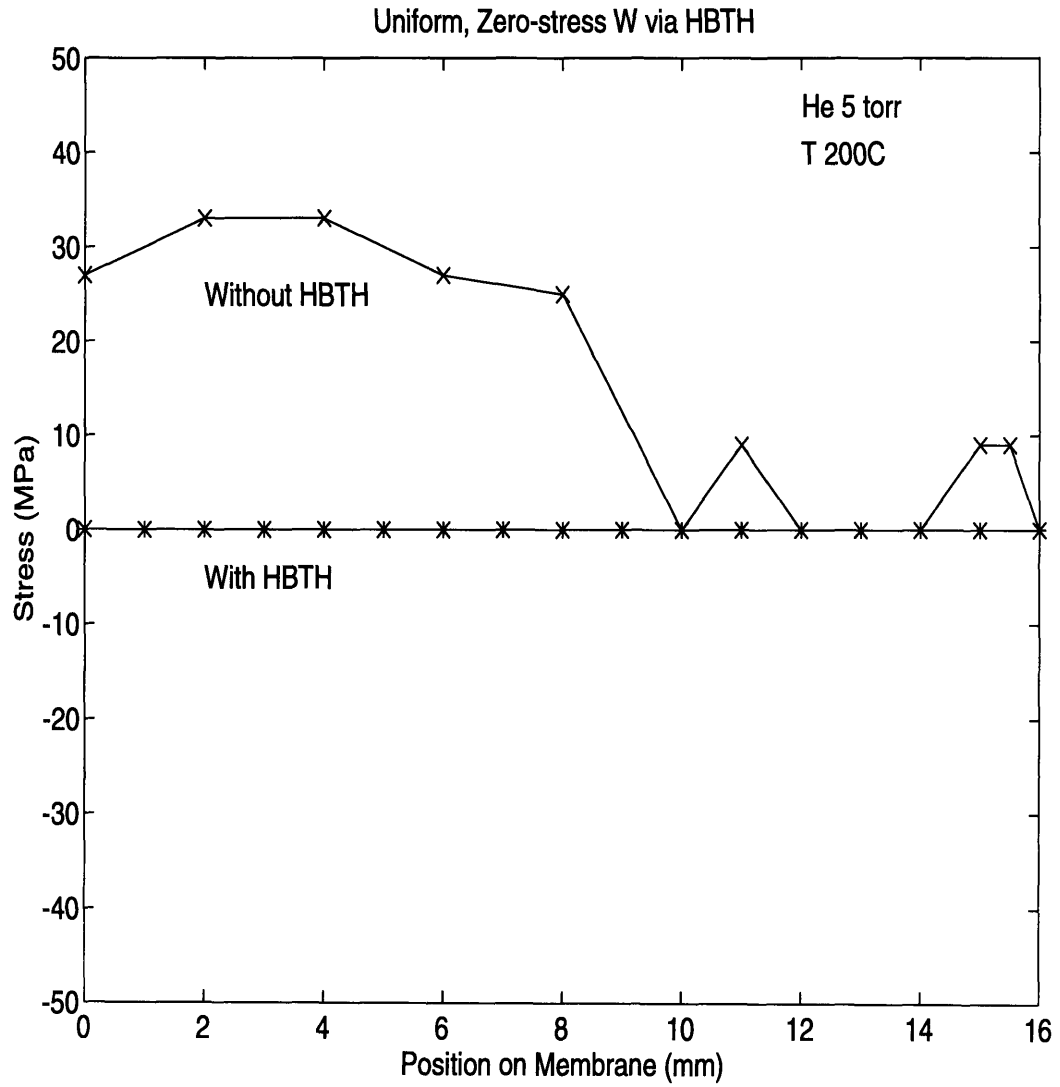
Figure 4-3: Unfirom, Zero-stress W via HBTH

4.3 Temperature Profile on Membrane

The model presented here is developed by Heinrich *et al* [5]. Symbols and values used in this section are listed below.

1. a thermal diffusion length.

2. T_{max} maximum temperature differential on the membrane.

3. $T_o = 473K = 200^\circ C$ temperature of the heat sink.

4. T temperature difference of the membrane relative to the heat sink.

5. $P_o = 0.1W/cm^2$ heat flux from plasma to membrane.

6. α_{rad} heat transfer coefficient due to radiation.

7. α_{He} heat transfer coefficient due to helium conduction.

8. $\alpha_{eff} = \alpha_{rad} + \alpha_{He}$ effective heat transfer coefficient.

9. $\lambda = 1.48W/cmK$ membrane thermal conductivity.

10. $\lambda_{He} = 1.436 \times 10^{-3}W/cmK$ helium thermal conductivity.

11. $d = 1\mu m$ thickness of the membrane.

12. $b = 3.1cm$ diameter of the membrane.

13. $d_{He} = 1mm$ distance of the gap between the membrane and mask holder.

14. $\epsilon = 1$ emissivity of membrane.

15. $\sigma = 5.6696 \times 10^{-8}Wm^{-2}K^{-4}$ Stefan-Boltzmann constant.

Among these values the thermal diffusion length and maximum temperature differential on the membrane are the most important in calculating the temperature profile on the membrane. The rest are necessary to derive these two values.

plasma heating

thermal radiation

conduction through helium
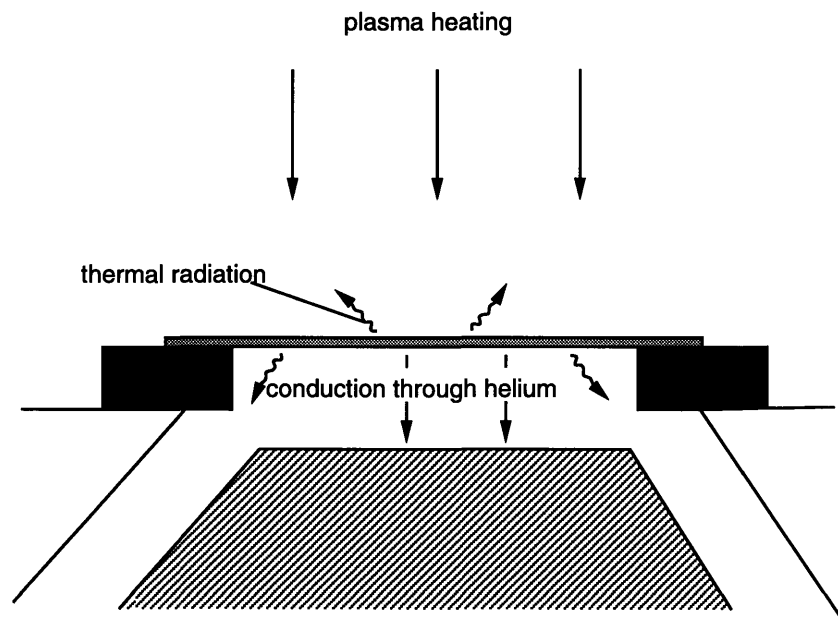
Figure 4-4: Heat Transfers in HBTH Setup
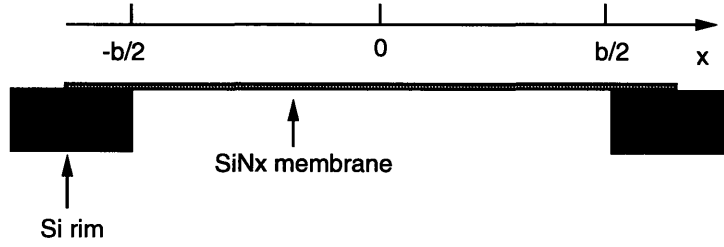
Figure 4-5: One Dimension Model for Heat Transfer

In the HBTH setup, the membrane dissipates heat by thermal radiation from surfaces and conduction through helium gas to the heat sink, as indicated in Figure 4.4. The heat flow and heat-transfer coefficients can be calculated.

(1) The heat flow due to thermal radiation is given by

$J_{rad} = \alpha_{rad}T$, where $\alpha_{rad} = 2(4\epsilon\sigma T_o^3)$ is the heat transfer coefficient assuming $T \ll T_o$.

(2) The heat flow from membrane to heat sink is given by

$J_{He} = \alpha_{He}T$, where $\alpha_{He} = \lambda_{He}/d_{He}$ is the heat transfer coefficient due to helium conduction.

Notice this is the same equation as Equation 4.1 in the new notation. The effective heat transfer coefficient is the sum of the radiation and conduction coefficients.

With these basic heat loss mechanisms in mind, we now consider the steady-state one dimensional case with a power distribution $P(x) = P_o$ for $-b/2 \le x \le b/2$ and $P(x) = 0$ elsewhere. The coordinates are defined as in Figure 4.5. The heat transfer differential equation for this case is given by

$$-a^2\frac{\partial^2 T}{\partial x^2} + T = \frac{P(x)}{\alpha_{eff}} \qquad (4.3)$$

where $a = (\lambda d/\alpha_{eff})^{1/2}$ is the thermal diffusion length. The boundary condition is $T(x = \pm\frac{b}{2}) = 0$. The solution of this temperature profile is

$$T(x) = \frac{P_o}{\alpha_{eff}}(1 - \frac{\cosh(x/a)}{\cosh(b/2a)}). \qquad (4.4)$$

26

The relevant coefficients are calculated below.

$$\alpha_{rad} = 2(4\epsilon\sigma T_o^3) = 4.7 \times 10^{-3} W/cm^2 K$$

$$\alpha_{He} = \lambda_{He}/d_{He} = 1.44 \times 10^{-2} W/cm^2 K$$

$$\alpha_{eff} = \alpha_{rad} + \alpha_{He} = 1.9 \times 10^{-2} W/cm^2 K$$

$$a = (\lambda d/\alpha_{eff})^{1/2} = 0.088 cm$$

$$T_{max} = T(x = 0) = 5K \ll T_o = 473K.$$

For comparison, the temperature profile is calculated without HBTH, where the only heat transfer is through radiation. The solution is the same as Equation 2.4 except for values α_{eff} and a.

$$\alpha_{eff} = \alpha_{rad} = 4.7 \times 10^{-3} W/cm^2 K$$

$$a = (\lambda d/\alpha_{eff})^{1/2} = 0.177 cm$$

$$T_{max} = T(x = 0) = 21K \ll T_o = 473K.$$

The two temperature profiles are plotted in Figure 4.6, which shows that without HBTH the center of the membrane has a much higher temperature than the edge of the membrane. The result is higher thermal stress in the center.

The graph shows that HBTH has two positive effects. First, it reduces the temperature differential by more than four times. Because thermal stress is directly proportional to the temperature on the membrane, reduction in the temperature differential during sputtering helps to reduce the thermal stress. Second, it produces a more uniform temperature profile across the membrane because of the reduced thermal diffusion length (a). A more uniform temperature profile minimizes the effect of high compressive stress at the edges as observed by Ku [13]. My results confirmed the above predictions because the stress measured on the membrane are uniform. Discussion of the results is in the next chapter.

The assumed emissivity of 1 is high. A more realistic value is probably around 0.2 [21]. Using $\epsilon = 0.2$ the temperature profiles are shown in Figure 4.7. We see that
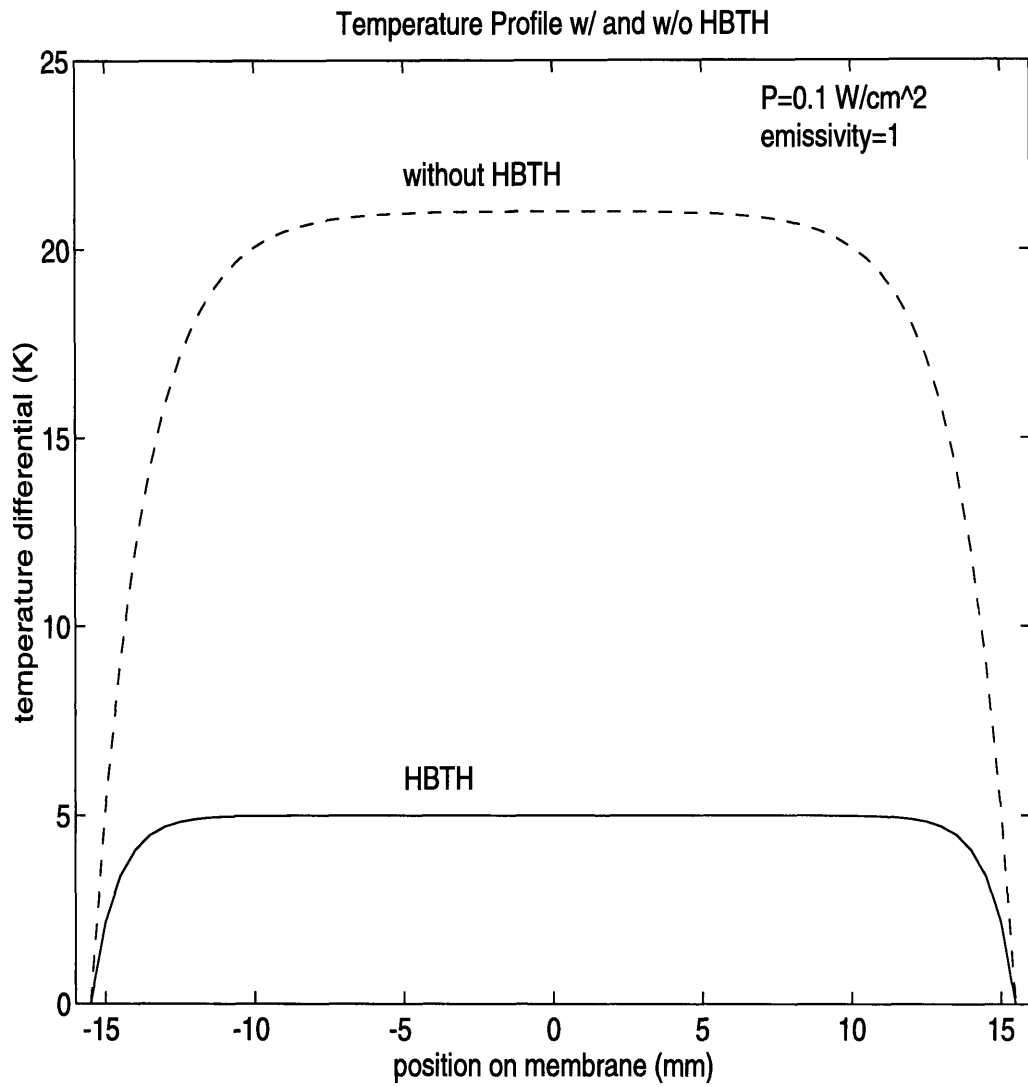
Figure 4-6: Temperature Profile of Membrane with High Emissivity

the effect of HBTH is much more dramatic in this case.
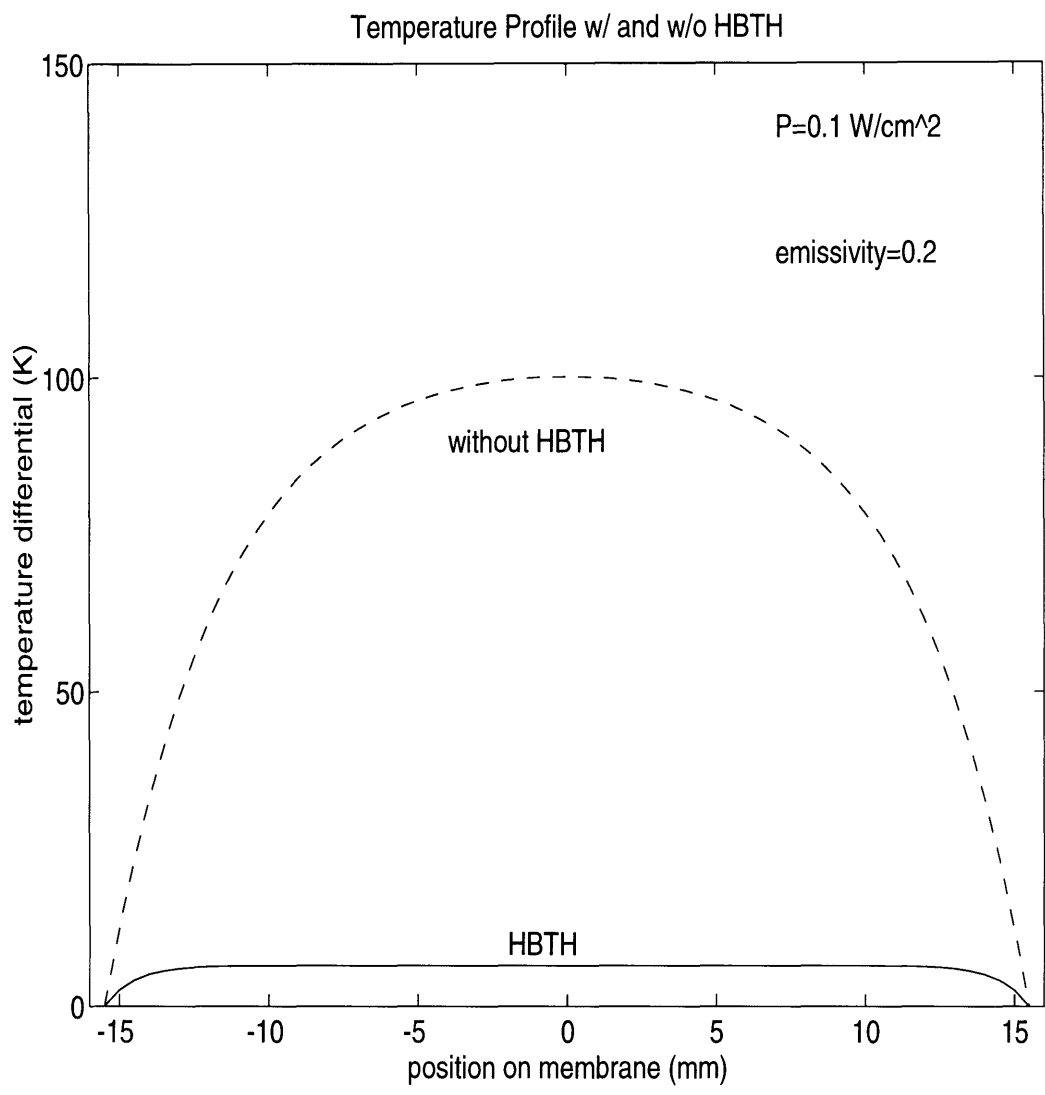
Figure 4-7: Temperature Profile of Membrane with Low Emissivity

Chapter 5

Measurement and results

5.1 Membrane Characterization

In order to measure the absorber stress, we need to know the thickness and intrinsic stress of the membrane. This section outlines the methods used for these measurements.

5.1.1 Membrane Thickness

The membrane thickness is obtained using a spectrometer which can measure the membrane transmission at different wavelengths. Since the transmission depends on the the membrane thickness and its optical properties, the measured data can be fitted to a relationship and the best fitting parameters contain enough information to calculate the thickness. Typical data and a fitting curve are shown below.

This technique was used in characterization of X-ray masks by Moel [16]. Gabrielle Owen improved this method and facilitated most of the thickness data used in this thesis [18].

5.1.2 Membrane Stress

A bulge test similar to the one used by Bromley is used to measure the stress of the membrane. It applies a differential pressure between the front and backside of the

31

Transmission Fit for MITa033

thickness=899.9 nm

n(632.8)=2.3434

k(632.8)=0.00628
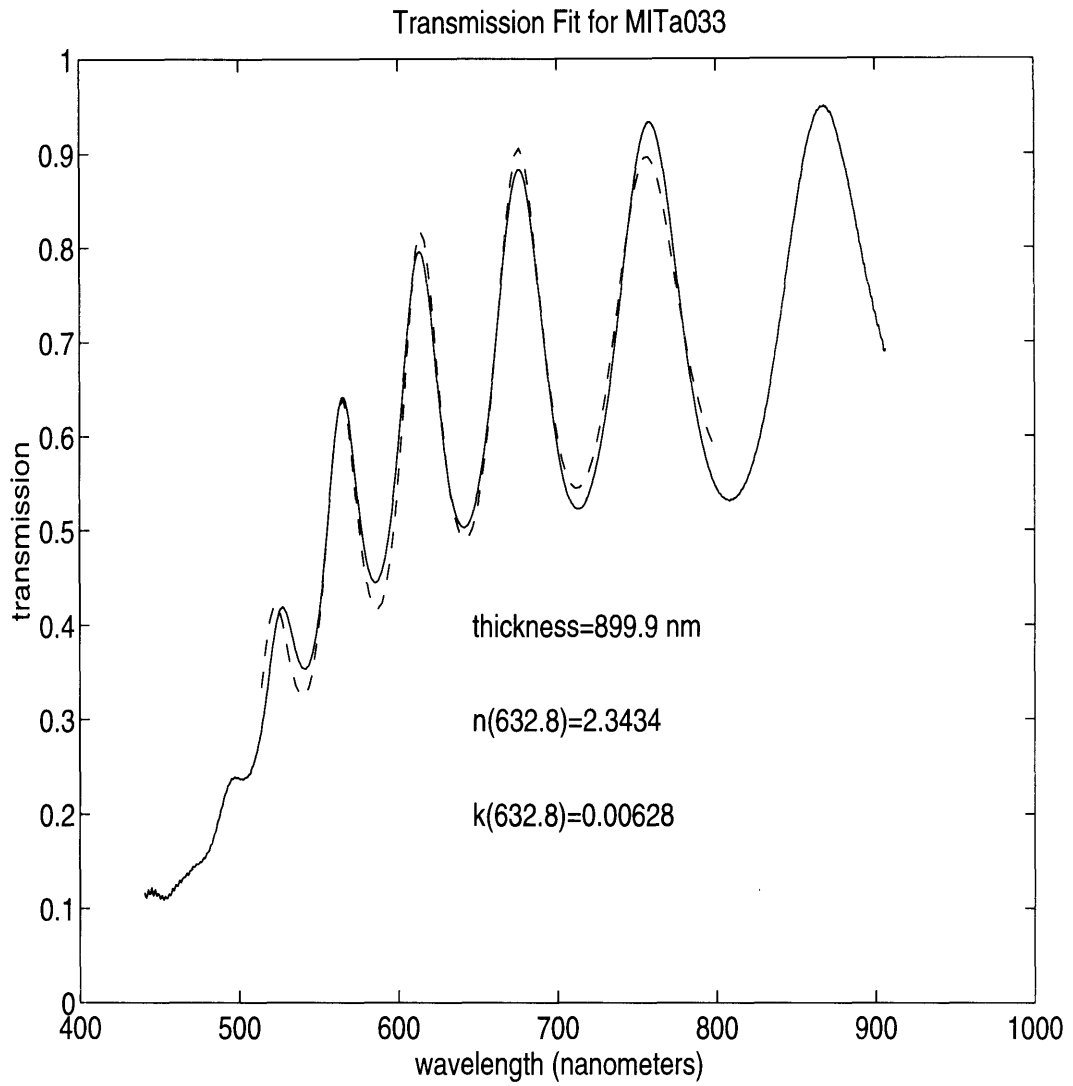
Figure 5-1: Data and Fitting Curve from Spectrometer
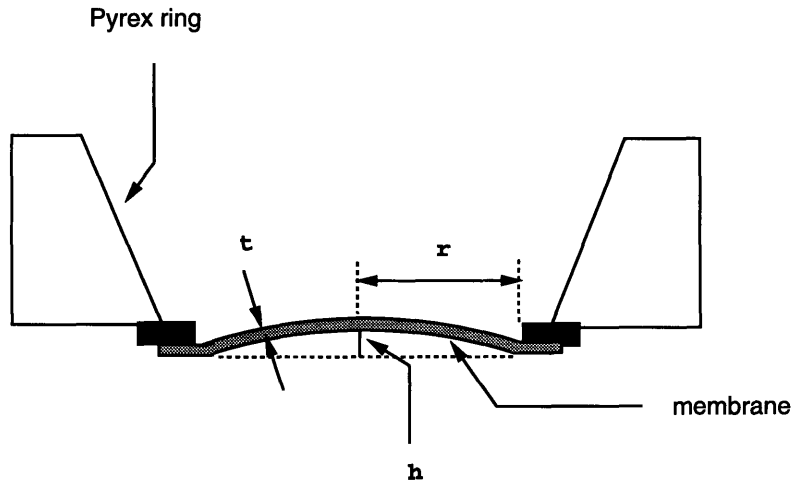
Figure 5-2: Bulge of Pressurized Membrane

membrane, and measures the resulting membrane bulge or deflection as depicted in Figure 5.2.

The amount of deflection at the center of the membrane can be used to measure its intrinsic stress. Bromley derived the following formula, using hoop stress formula on a circular membrane and assuming the deflection is small,

$$p = \frac{4t\sigma_s}{r^2}h + \frac{8t}{3r^4}\frac{E}{1-\gamma}h^3 \tag{5.1}$$

where t, r, h, σ_s, $\frac{E}{1-\gamma}$ are the thickness, radius, deflection, intrinsic stress and bulk modulus of the membrane, and p is the differential pressure applied [1].

Since t and r are known, σ_s and $\frac{E}{1-\gamma}$ can be determined by measuring h at various p's and fit the data to the above formula.

This technique can be extended to measure stress in films deposited on a membrane by measuring the properties of the composite layers. In addition, it may be used in a *in situ* stress control setup because it measures the stress non-destructively. This possibility is explored in chapter 6.
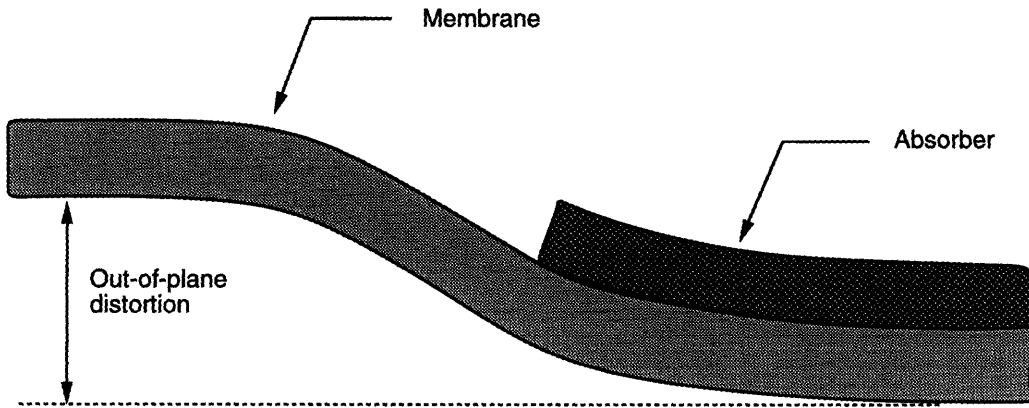
Figure 5-3: Membrane Out-of-Plane Distortion

5.2 Absorber Stress

In this section, absorber stress is measured using a substrate bending model. First, the equation of absorber stress is introduced. Then, the process involved in the measurement is described.

5.2.1 Out-of-plane Distortion and Absorber Stress

Yanof's model of membrane deflection due to the bending from the absorber stress and membrane intrinsic stress is used to derive the following relationship for an X-ray mask half covered with absorber,

$$\sigma_a = \frac{2\sigma_s \eta}{t_a(1 + \frac{t_a}{t_s})} \tag{5.2}$$

with an absorber stress of σ_a and thickness t_a, membrane stress of σ_s and thickness t_s, and total out-of-plane deflection of η[13] [26]. Since δ_s, t_s and σ_a are determined from the techniques described in last section, we can calculate σ_a by measuring η and t_a . A cross-section view of out-of-plane distortion η is given in Figure 5.3.

The X-ray mask half covered with absorber is made using a photolithography process described in the next section. Its out-of-plane distortion is measured using a

Linnik interferometer.

5.2.2   Photolithography Process

The absorber film (W and Cr) is sputtered on an X-ray mask using the HBTH setup in chapter 4. To make an X-ray mask half covered with absorber, a photolithography technique is used. This process is illustrated in Figure 5.4.

The X-ray mask is RCA cleaned to remove organic contamination. Then a thin Cr adhesion layer ($10nm$) and a W absorber layer ($500nm$) are sputter-deposited on the membrane. The membrane is then coated with photo resist (1822) and oven baked. The next step is to expose the resist on half of the membrane using UV light. The exposed resist is then washed off with a developer. The final step are W and Cr etching and removing the remaining resist.

The top view shows that half of the mask is covered with absorber. The interface between the absorber and the membrane is a step with height equaling the thickness of the absorber. This mask is then put under the Linnik interferometer to measure the step height and out-of-plane distortion.

5.3   Result and Analysis

To test the helium backside temperature homogenization method, a number of sputtering experiments on a single membrane as well as on different membranes were carried out. If the absorber stress is uniform, then HBTH is successful.

During these depositions, helium was flowed at a fixed pressure in the small gap between the membrane and the mask holder to homogenize the temperature of the membrane. A detailed explanation of the setup was presented in chapter 4.

The sputtering system used was a MRC 8620 upgraded with a new Cryo pump and a new Cr target. The base pressure before sputtering was below $3 \times 10^{-6} torr$. Working gas was Argon (Ar). The pressure range tested was from $16.85 mtorr$ to $20 mtorr$. Membrane temperature was kept at $200^{\circ}C$ to ensure the stable α phase W [13]. RF power applied was $200W$, and peak-to-peak voltage was $1.5KV$. Pre-sputtering on

SiNx Membrane

Frontside

Backside

W/Cr

1) Sputter W/Cr

Photo Resist

2) Spin coat photo resist and bake

UV light

3) UV expose half of membrane

4) Develop exposed resist and etch W/Cr

Step

5) Expose and develop the rest of the resist

SiNx membrane

W/Cr

Optically flat Pyrex ring

Top View

X-ray mask half covered with absorber
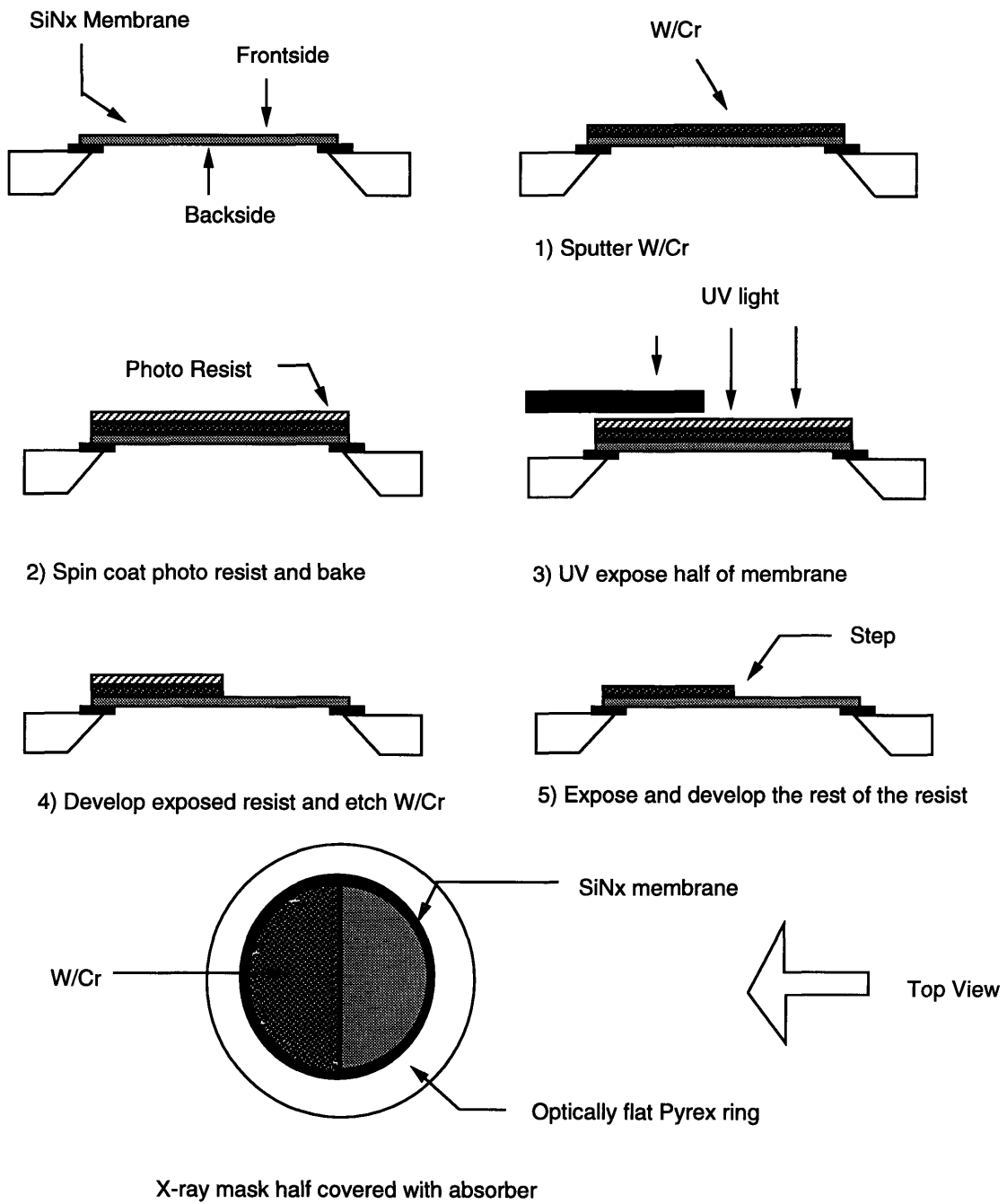
Figure 5-4: Photolithograph Process

the shutter was done for 5 minutes to clean the targets from any oxidization.

After one month of continuous sputter runs in an effort to find the zero-stress Ar pressure and data for stress at different pressures, I got the following results.

Data show that very low stress tungsten absorber over an entire membrane can be produced with the HBTH, which proves that our approach is correct. Unfortunately, the low stress is not readily reproducible. At Ar Pressure of $19.92mtorr$, zero-stress W was produced; however, the sputter runs at the same pressure failed to obtain the same stress.

Nonetheless, all HBTH data consistently show a uniform stress over the entire membrane, as shown in Figure 5.5. Notice that when the stress is tensile, the uniformity is very good except for one. The exception is the data with an upward tilt at the edge of the membrane. Since the normal thermal gradient induced stress nonuniformity should be lower at the edge, this is probably an error in measurement.

Figure 5.6 summarizes the thickness of tungsten at different Ar pressures. The error bar in thickness is $\pm 15nm$, since that is the accuracy of the Linnik interferometer. And Figure 5.7 gives the relationship between stress and pressure. Its error bar is calculated by setting $\Delta \eta = 15nm$ and use the formula

$$\Delta \sigma_a = \frac{2\sigma_s \Delta \eta}{t_a(1 + \frac{t_a}{t_s})}.$$

(5.3)

It shows the stress value at any pressure is not reproducible. Data for these two figures are summarized in Table 5.1.

In chapter 3, we listed working gas (Ar) pressure, electric power, substrate temperature, base pressure, and geometry of the vacuum chamber as important deposition conditions which influence the absorber stress. Because working gas (Ar) pressure, RF power, membrane temperature, and base pressure in the sputter experiments were satisfactorily controlled, the uncertain parameters left are the geometry of the vacuum chamber. Since sputtering is in a plasma environment, the chamber geometry can have a significant effect on the stress of the absorber.

Nonetheless, the goal of building and characterizing the helium backside tem-
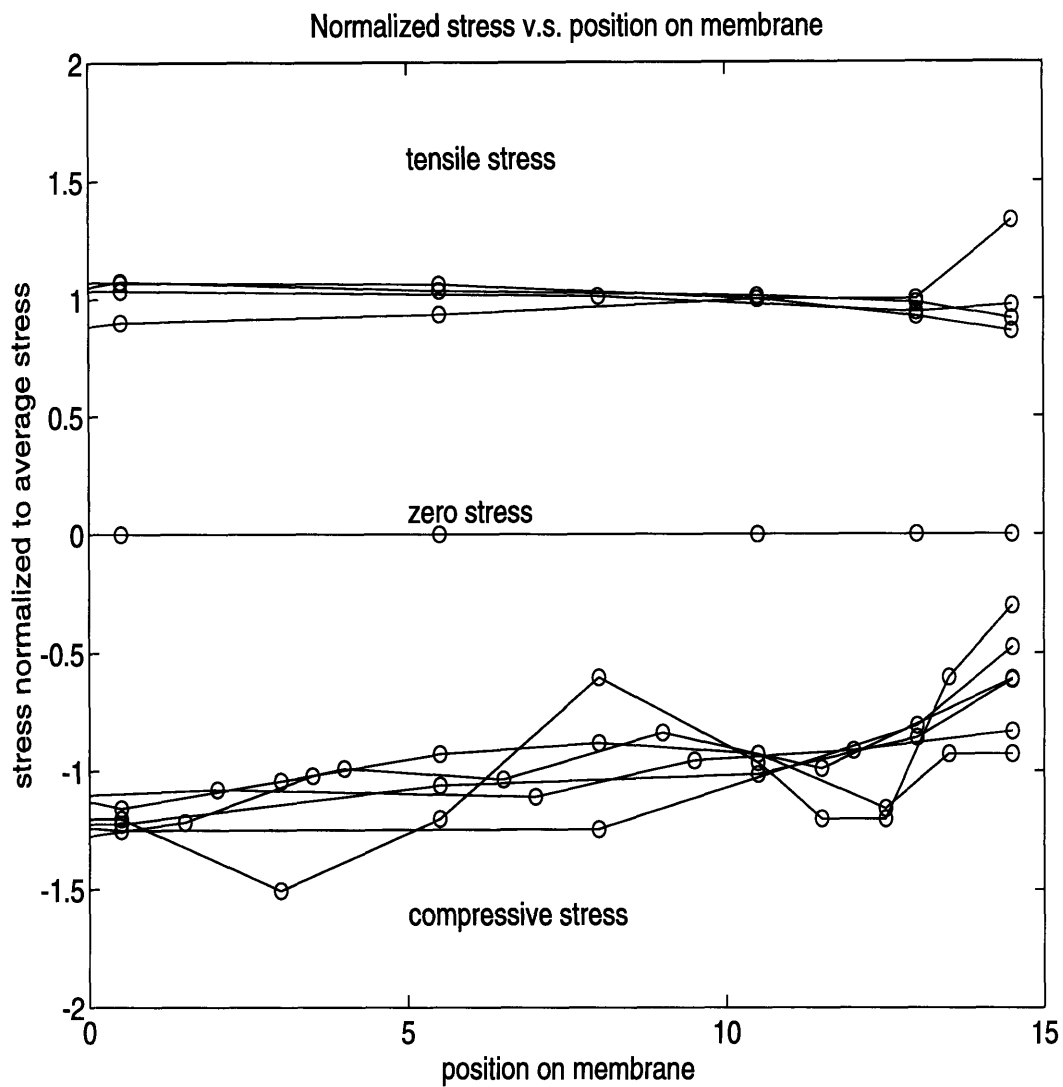
Figure 5-5: Normalized Absorber Stress on Membrane

Table 5.1: W Stress Data

Ar Pressure (mtorr)	Absorber Stress (MPa)	Stress Error (MPa)	Absorber Thickness (nm)	Membrane Stress (MPa)	Membrane Thickness (nm)
17.25	-233.5	33.6	519	850	1123
17.29	-308.9	36.6	486		
17.29	-445.6	35.6	497		
17.36	-519.5	32.9	527		
19.76	-349.2	7.7	521	210	918.1
19.92	-442.9	7.7	520		
19.92	0	7.6	526		
19.92	389.6	8.8	473		
19.92	234.6	7.7	521		
20	74.3	7.4	538		
20	298.9	6.9	565		

perature homogenization scheme with a tungsten absorber on an X-ray mask has been accomplished with the above experiments. Due to the poor reproducibility of low stress tungsten absorber, an *in situ* monitor scheme is probably a good way to improve this situation.

Pressure v.s. Absorber Stress
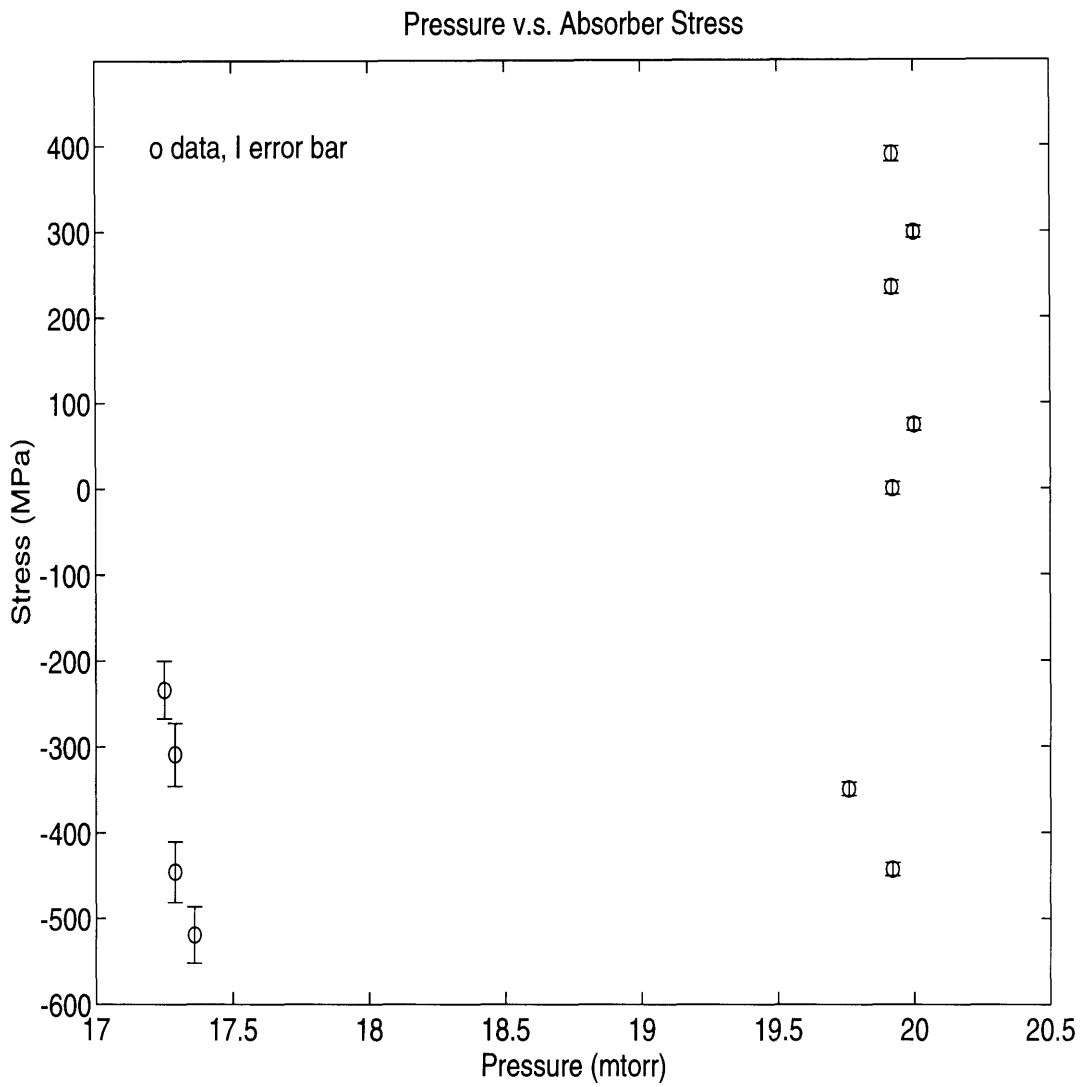
Figure 5-6: Absorber Stress and Pressure Curve
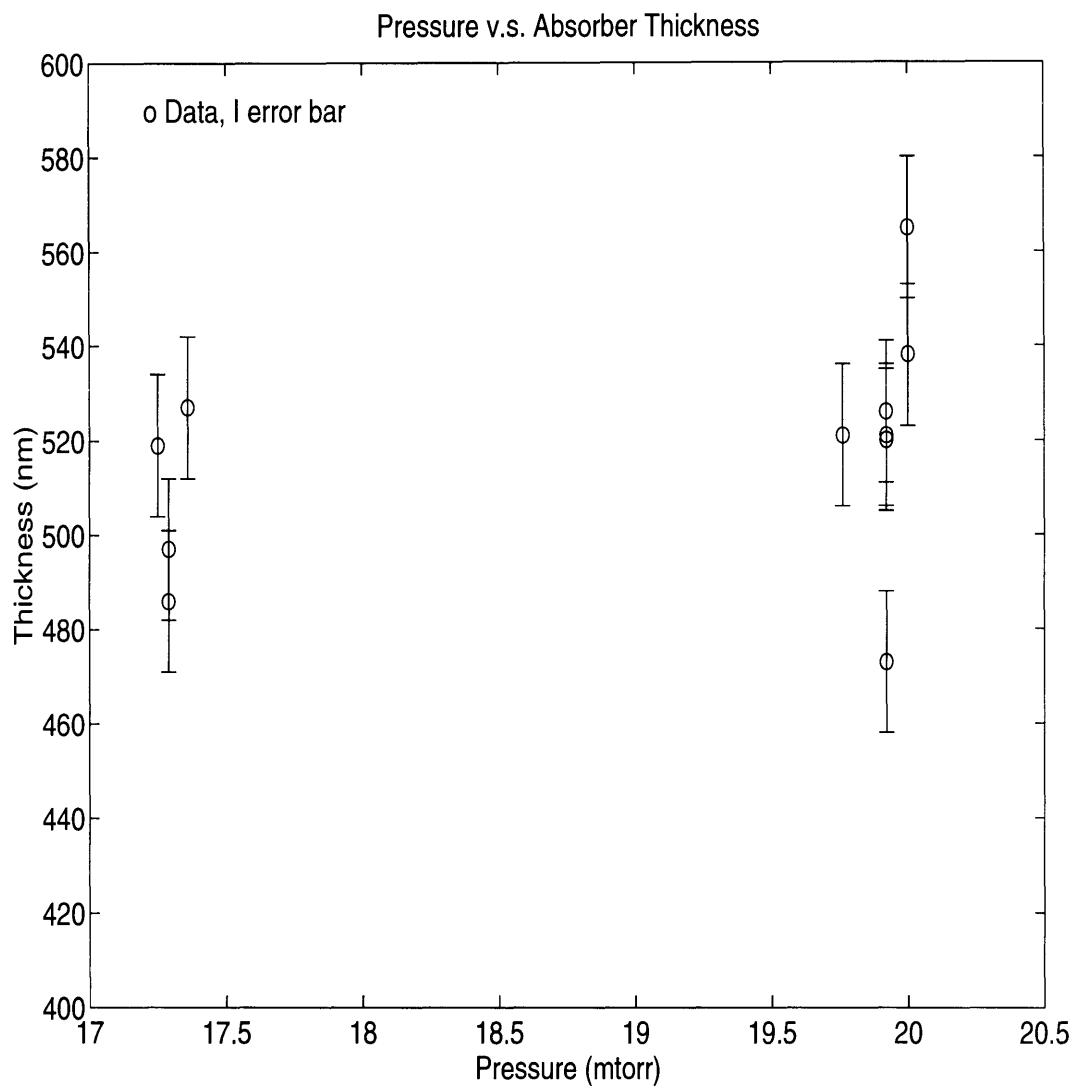
Figure 5-7: Absorber Thickness and Pressure Curve

Chapter 6

Future Works

So far, we have been using open-loop control in the sputtering experiments. Because these experiments failed to produce repeatable results, we need to consider an *in situ* closed-loop control method.

In an open-loop control system, desired results are obtained by successfully controlling all the relevant experimental parameters, which have non-negligible influence on the final results, i.e. stress. Therefore, the task of open-loop control is primarily to discover these parameters, their proper values, and maintain them to produce repeatable results. There are two shortcomings associated with this method.

First, the task of discovering all of the relevant parameters and to find the best combination of values can be very difficult, especially when many parameters are involved and some of them are unknown or hard to control. In these cases, closed-loop control becomes preferable because it can be accomplished by involving fewer parameters and a control feedback. These parameters are varied during the experiment by the feedback control to keep the stress low.

Second, the experimental results from an open-loop system are not known with certainty until the deposition is completed and the W stress is measured directly, for example by interferometry. On the other hand with a closed-loop *in-situ* control method, the stress can be detected and adjusted to the desired value during deposition.

From the above discussion, a closed-loop system can measure the film stress in

real time and use it as feedback control signals. One such *in situ* monitor scheme was developed by Ku [14]. As mentioned earlier in chapter 4, the theory involved in the bulge test can be applied to *in situ* control as discussed in the next section.

6.1 *In situ* Stress Control in W Deposition

The Bromley stress formula can be extended for multi-layer films as shown below,

$$p = \frac{4}{r^2}h(\sigma_o t_o + \sigma_1 t_1) + \frac{8}{3r^4}h^3(\frac{E_o}{1-\gamma_o}t_o + \frac{E_1}{1-\gamma_1}t_1), \qquad (6.1)$$

where the subscript '$_o$' represents membrane parameters and the subscript '$_1$' represents W parameters. We now analyze how this formula can be used for *in situ* stress control in W deposition.

First, $\frac{E_o}{1-\gamma_o}$, t_o, σ_o and $\frac{E_1}{1-\gamma_1}$ are constant parameters unrelated to deposition conditions. The first three are membrane parameters and can be measured with the bulge tester and the spectrometer in the lab. The Young's modulus of W is $E_1 = 3.45 \times 10^{11} Pa$ [22] and $\gamma_1 = 0.28$ [18].

Second, the pressure p is the pressure of helium, which is set at $5 torr$. Since our goal is to produce zero-stress W, σ_1 is also fixed at zero.

The only variables left undetermined are deflection h and W thickness t_1. The relationship between h and t_1 is key for *in situ* stress control. Figure 6.1 shows a typical relationship between h and t_1 from Equation 6.1, assuming reasonable values for the parameters. This curve is called the ideal curve or target curve. The ideal curve is bounded by the allowable error in stress $\pm 5 MPa$.

During sputter deposition W thickness t_1 and the corresponding actual membrane deflection h' can be monitored using a "thin film thickness monitor" and a photonic sensor, respectively. The difference between the measured h' and ideal h can be used as a feedback signal to adjust the Ar pressure until the measured h' falls on the target curve. Therefore by controlling membrane deflection *in situ* we can effectively control the W stress during deposition. A schematic based on the above discussion is shown in Figure 6.2.

Calculated Deflection v.s. W thickness
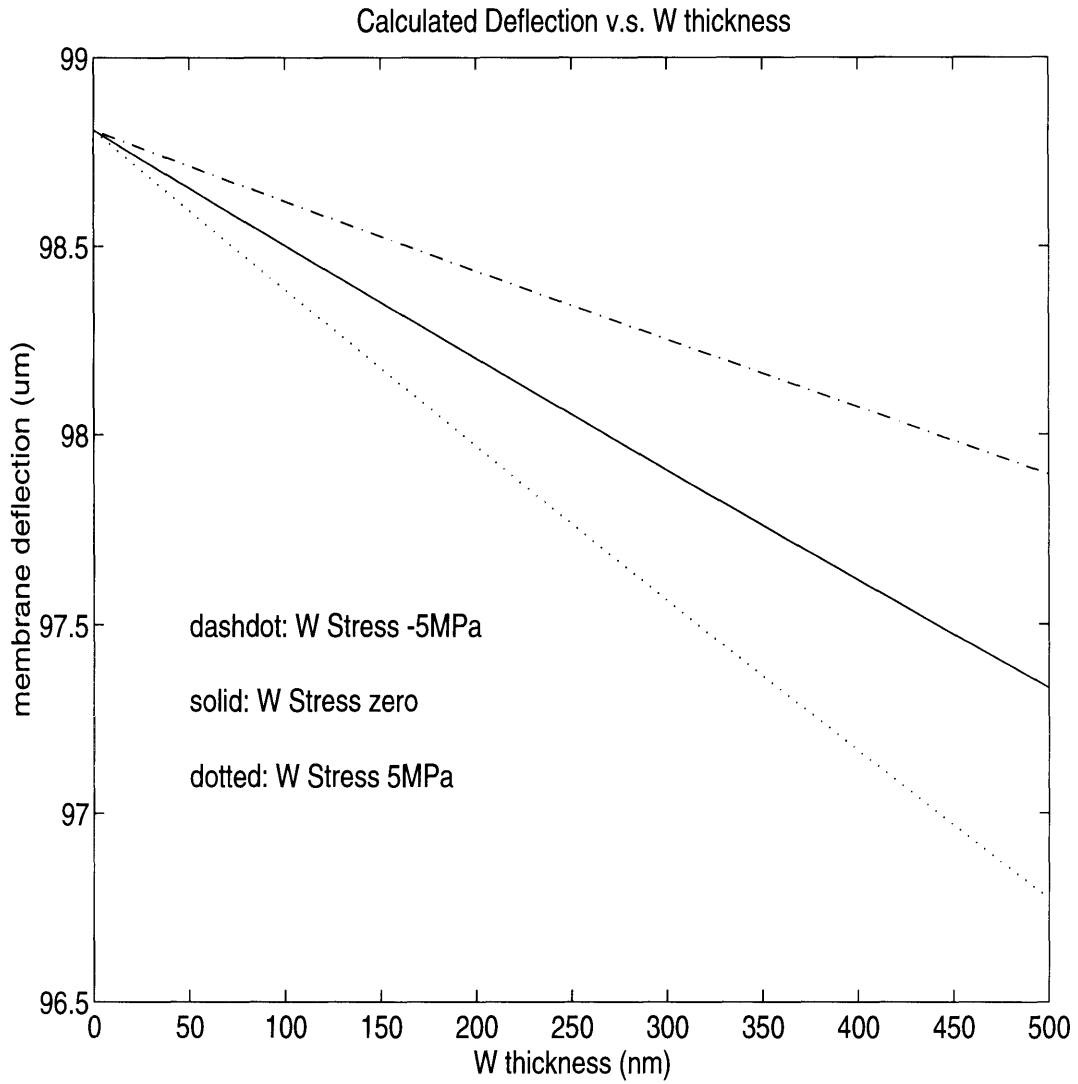
Figure 6-1: Target Curve for *in situ* Control
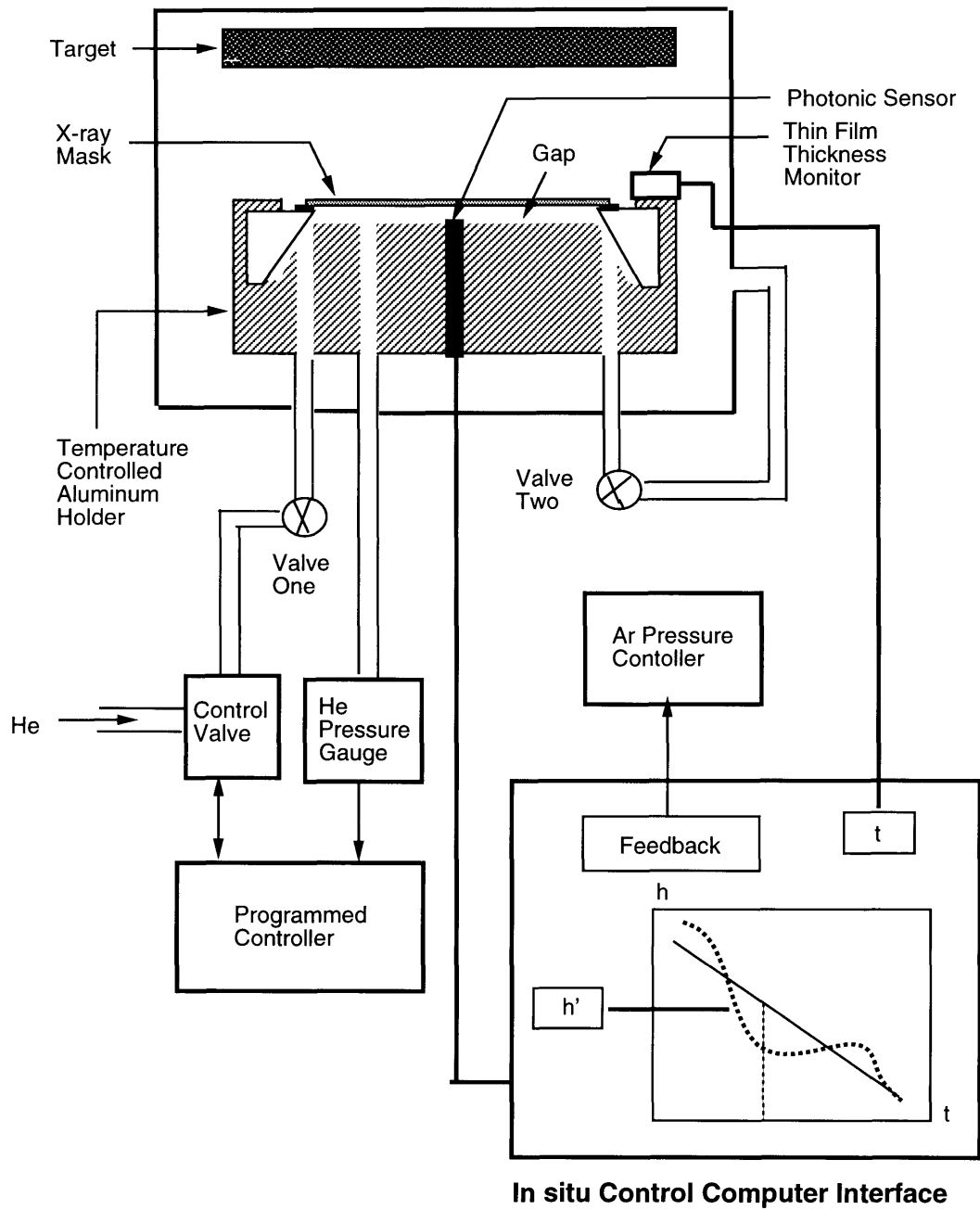
Figure 6-2: Schematics for *in situ* Control

6.2 Practical Issues

Outlined below are some considerations that may be involved if such a scheme is to be implemented. The key question is the accuracy of the photonic sensor measurements. From Figure 6.1, we need a sensor sensitivity of $\pm 0.5 \mu m$ to ensure that W stress is below $\pm 5 \times 10^7 dyn/cm^2 = 5MPa$ at $500nm$.

Since the mask holder and the sensor are heated to $200^\circ C$, the measured data could be skewed due to thermal expansion. This means that the target curve must be adjusted with experimental values.

Moreover, the deflection we want to measure is the one at the center of the membrane, while the photonic sensor may not be centered. This error can be a problem.

In Figure 6.3, h $(= 100 \mu m$ from Figure 6.2) is the center deflection we want to measure; however, the photonic sensor is off center so we actually measured h'. Assume $a = 2mm$ is the error in centering and $b = h - h'$ is the resulted error in measured deflection. $r = 31/2mm$ is the membrane radius and R is the radius of the bow. Some simple geometrical manipulations show that

$$
\begin{aligned}
R &= \frac{h^2 + r^2}{2h} = 1201.3mm, \\
b &= R - \sqrt{R^2 - a^2} = 0.0017mm = 1.7\mu m.
\end{aligned}
$$

Since the allowable error of the measurement is only $\pm 0.5 \mu m$, a $1.7 \mu m$ error is serious. One way to get around this problem is to measure the deflection of membrane before deposition, calculate the centering error a, and use it in subsequent deflection measurements to convert h' to h.

Figure 6.4 shows a better solution for *in situ* control, where four photonic sensors are used instead of just one. If we assume that we know the accurate positions of the four photonic sensors relative to each other, then their four measurements will determine the radius of the hemisphere. Since the radius of the membrane is known, the deflection at the center of the membrane can be calculated. This approach has the advantage of eliminating the photonic sensor off-center error.
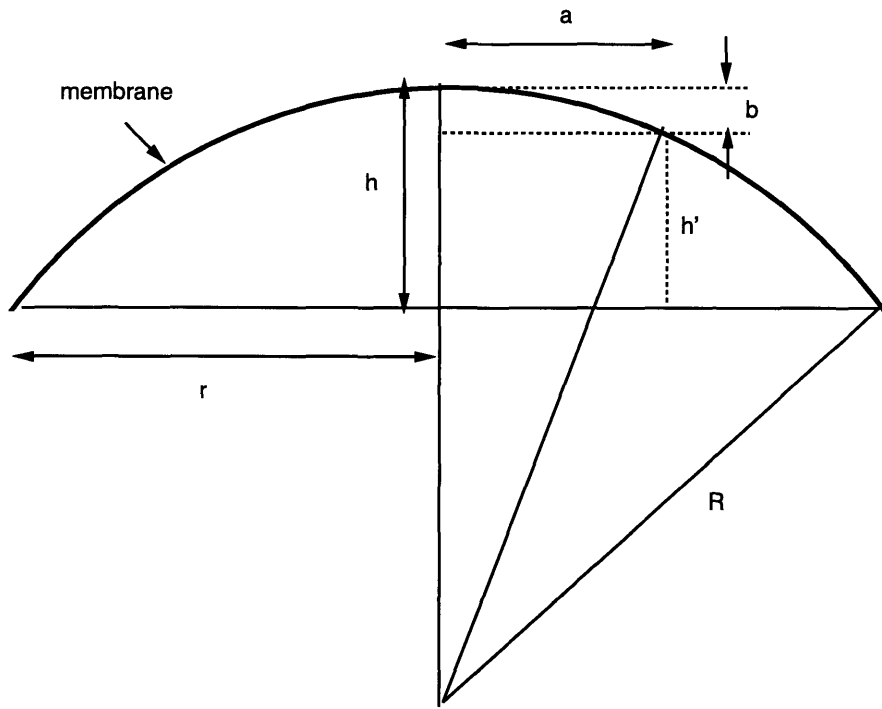
Figure 6-3: Deflection Error due to Photonic-sensor Off-center
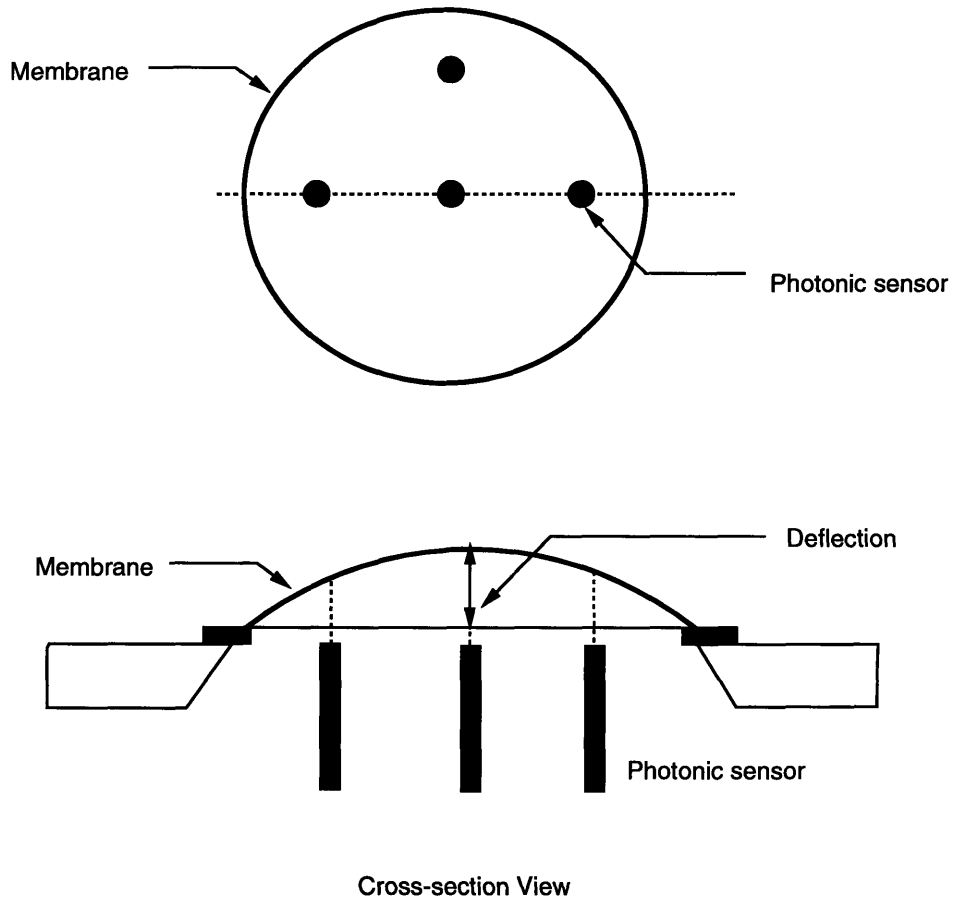
Figure 6-4: *In situ* Control with Four Photonic-sensors

Appendix A

Tungsten Sputter Run Sheet

1. RCA clean mask.

2. close high vacuum valve.

3. vent chamber with N_2 to atomerspher pressure.

4. open chamber and load membrane.

5. close chamber.

6. rough out chamber to $50mtorr$.

7. open high vacuum valve.

8. turn on water valve for cooling target.

9. turn on heater for the mask holder.

10. wait till base pressure is low ($\leq 2^{-6}torr$.

11. flow He till its pressure stabilizes at $5torr$.

12. flow Ar and close high vacuum valve almost all the way, leave one and half to two turns.

13. turn on Main power, wait till the "Ready/Off" button lights up (green).

14. glow start plasma, adjust power to set level (e.g. 200 W).

15. pre-sputter on shutter for 5 mins.

16. sputter Cr for 1 min.

17. power off by push"Ready Off" button.

18. switch target to W.

19. pre-sputter on shutter for 5 mins

20. sputter W for 25 mins.

21. power off by push"Ready Off" button.

22. wait about 5 mininus.

23. turn off heater.

24. turn off Ar.

25. turn off He.

26. leave the water running till the system cools down.

27. vent chamber and take mask out.

Appendix B

Making a Mask Half-covered with Absorber

(a) sputter W/Cr on mask.

(b) set the spinner at 3,000RPM and 30sec.

(c) spin photon resist 1822 on mask.

(d) oven bake at $90^\circ C$ for 25mins.

(e) prepare developer 351.

(f) let mask cool for 5mins.

(g) cover half of the membrane with a celeved half Si wafer.

(h) UV exposure for 2mins on Tamrrack.

(i) develop the exposed resist with developer 351.

(j) rainse with DI water.

(k) etch W for 15 to 25mins.

(l) rainse with DI water.

(m) etch Cr for 2mins.

(n) rainse with DI water.

(o) UV exposure for 2mins.

(p) develop the remaining resist.

(q) rainse with DI water.

(r) N_2 dry.

Bibliography

[1] E.I. Bromley, J.N. Randall, D.C. Flanders, and R.W. Mountain. A technique for the determination of stress in thin films. *J. Vac. Sci. Technol.*, B1(4):1364–1366, October 1983.

[2] M. Chaker, S. Boily, Y. Diawara, M. A. EI Khakani, E. Gat, A. Jean, H. Lafontaine, H. Pepin, J. Voyer, J. C. Kieffer, A. M. Haghiri-Gosnet, F.R. Ladan, M. F. Ravet, Y. Chen, and F. Rousseaux. X-ray mask development based on sic membrane and w absorber. *J. Vac. Sci. Technol.*, B10(6):3191–3195, November 1992.

[3] Kasturi L. Chopra. *Thin Film Phenomena*, chapter 2.2. McGraw-Hill Book Company, 1969.

[4] Saul Dushman. *Scientific Foundations of Vacuum Technique*, page 48. New York London, Joh Wiley & Sons, Inc., 2nd edition.

[5] K. Heinrich, H. Betz, and H. Heuberger. Heating and temperature-induced distortion of silicon x-ray masks. *J. Vac. Sci. Technol.*, B1:1352–1357, October 1983.

[6] A. Heuberger. X-ray lithography. *J. Vac. Sci. Technol.*, B6(1):107–121, January 1988.

[7] Masamitsu Itoh and Masaru Hori. An ultra-low stress tungsten absorber for x-ray masks. *J. Vac. Sci. Technol.*, B9(1):165–168, January 1991.

[8] Masamitsu Itoh, Masaru Hori, and Soichi Nadahara. The origin of stress in sputter-deposited tungsten films for x-ray masks. *J. Vac.*

Sci. Technol., B9(1):149–153, January 1991.

[9] K. Kadela, W. K. Schomburg, and G. Stern. X-ray masks with tungsten absorbers for use in the liga process. *Microelectronic Engineering*, 21:123–126, 1993.

[10] Toshihiko Kanayama, Minoru Sugawara, and Junji Itoh. Reduction in x-ray mask distortion using amorphous wnx absorber stress compensated with ion bombardment. *J. Vac. Sci. Technol.*, B6(1):174–177, January 1988.

[11] Monty King and Peter Rose. Experiments on gas cooling of wafers. *Nuclear Instruments and Methods*, 189:169–173, 1981.

[12] R.R. Kola, G.K. Celler, C.W. Frackoviak, and L.E. Trimble. Stable low-stress tungsten absorber technology for sub-half-micron x-ray lithography. *J. Vac. Sci. Technol.*, B9(6):3301–3305, November 1991.

[13] Yao-Ching Ku. *Fabrication of Distorion Free x-ray Masks Using Low Stress Tungsten*. Ph.D. Thesis, MIT EECS, Cambridge, MA, 1991.

[14] Y.C. Ku, Lee-Peng Ng, Roger Carpenter, Kenneth Lu, Henry I. Smith, L.e. Hass, and I. Plotnik. In situ stress monitoring and deposition of zero-stress w for x-ray masks. *J. Vac. Sci. Technol.*, B9(6):3297–3300, November 1991.

[15] H. Li, M. Mondol, G. Owen, and H. I. Smith. Uniform, zero-stress w via he-backside temperature stabilization. *International Symposium on Electron, Ion and Photon Beams*, June 1994.

[16] A. Moel, W. Chu, K. Early, Y.-C. Ku, E. E. Moon, F. Tsai, Henry I. Smith, M. L. Schattenburg, C. C. Fung, Griffith F. W., and L. E. Hass. Fabrication and characterization of high-flatness mesa-etched silicon nitride x-ray mask. *J. Vac. Sci. Technol.*, B9(6):3287–1021, 1991.

[17] M. Nakaishi, M. Yamasda, and M. Nakamura. Backside helium cooling of x-ray masks in reactive ion etching process. *Proc. of 1989 Intern.*

Symp. on MicroProcess conference, pages 99–103.

[18] Gabrielle Owen. *Optical and Mechanical Characterization of Thin Membranes for X-Ray Lithography*. M. Eng. Thesis, MIT EECS, Cambridge, MA, May 1994.

[19] Peter D. Parry. Target heating during ion implantation. *J. Vac. Sci. Technol.*, 13(2):622–629, March 1976.

[20] Peter D. Parry. Localized substrate heating during ion implantation. *J. Vac. Sci. Technol.*, 15(1):111–115, January 1978.

[21] G. Rittenhouse. Private communications. September 1993.

[22] Robert B. Ross. *Metallic Materials Specification Handbook*, page 611. E. & F. N. Spon, 3rd edition, 1980.

[23] K. Suzuki and Y. Shimizu. X-ray mask technology: Low-stress tungsten deposition and sub-half-micron absorber fabrication by single-layer resist. *Microelectronic Engineering*, 14:207–214, 1991.

[24] Alan D. Wilson. X-ray lighography: Can it be justified. *SPIE Vol 537 Electron-Beam, X-Ray, and Ion-Beam Techniques for Submicrometer Lithographies*, IV:85–101, March 1985.

[25] Hideki Yabe, Kenji Marumoto, Sunao Aya, Nobuyuki Yoshioka, Takeshi Fujino, Yaichiro Watakabe, and Yasuji Matsui. Sputtered w-ti film for x-ray mask absorber. *Jpn. J. Appl. Phys.*, 31(12B):4210–4214, 1992.

[26] Arnold W. Yanof, Douglas J. Resnick, Constance A. Jankoski, and William A. Johnson. X-ray mask distortion: process and pattern dependence. *SPIE Vol. 632 Electron-Beam, X-Ray, & Ion-Beam Techniques for Submicrometer Lithographies*, V:118–132, 1986.